IEEE Photonics Journal
An IEEE Photonics Society Publication

Open Access

Outage Analysis of Mixed FSO/WiMAX Link

Volume 8, Number 1, February 2016

Nemanja Zdravković, Student Member, IEEE
Milica I. Petkovic, Student Member, IEEE
Goran T. Djordjevic, Member, IEEE
Kimmo Kansanen, Member, IEEE

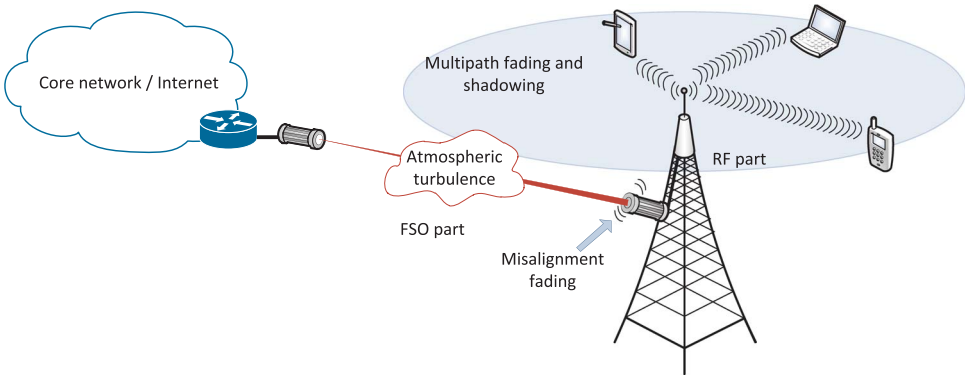

DOI: 10.1109/JPHOT.2016.2516250
1943-0655 © 2016 IEEE

IEEE photonics SOCIETY

IEEE

Outage Analysis of Mixed FSO/WiMAX Link

**Nemanja Zdravković,[1,2] *Student Member, IEEE*,
Milica I. Petkovic,[2] *Student Member, IEEE*,
Goran T. Djordjevic,[2] *Member, IEEE*, and Kimmo Kansanen,[1] *Member, IEEE***

[1]Department of Electronics and Telecommunications, Norwegian University of Science and Technology, 7491 Trondheim, Norway
[2]Department of Telecommunications, Faculty of Electronic Engineering, University of Niš, 18000 Niš, Serbia

DOI: 10.1109/JPHOT.2016.2516250

Manuscript received September 27, 2015; revised December 21, 2015; accepted January 4, 2016. Date of publication January 8, 2016; date of current version January 20, 2016. This work was supported in part by the Norwegian Ministry for Foreign Affairs through the project "Norwegian, Bosnian, and Serbian cooperation platform for university and industry ICT R&D" and in part by the European COST Action IC1101 Optical Wireless Communications—An Emerging Technology (OPTICWISE). Corresponding author: G. T. Djordjevic (e-mail: goran@elfak.ni.ac.rs).

Abstract: In this paper, we study the outage performance of a complex system consisting of a free-space optical (FSO)/radio-frequency (RF) link. Using radio over free-space optics technology, the FSO link carries Worldwide Interoperability for Microwave Access (WiMAX) signals from a core network to a WiMAX base station, delivering traffic to multiple end RF users. A novel closed-form analytical expression for overall outage probability is derived when *M*-ary phase-shift keying (*M*-PSK) and *M*-ary quadrature amplitude modulation (*M*-QAM) are applied. The analysis is performed when the FSO link is under the influence of the Gamma–Gamma turbulence, path loss, and misalignment between the transmitter and receiver apertures, and the RF part is influenced by the Gamma-shadowed Nakagami-*m* multipath fading. To illustrate the usefulness of the derived expressions, we present some numerical results that enable us to estimate the effects of different transceiver and channel parameters on the outage probability. The results are used for optimizing the transmitter laser beam radius at the waist to achieve the minimal overall outage probability in the case of different conditions over the RF part. The numerical and simulation results show that multipath fading severity and shadowing spread over the RF part have a significant effect on the optimal value of the laser beam waist and can decrease the overall outage probability for several orders of magnitude.

Index Terms: Atmospheric turbulence, fading, free space optics, outage probability, pointing errors, shadowing, Worldwide Interoperability for Microwave Access (WiMAX).

1. Introduction

Radio over free-space optics, containing optical carriers modulated in an analog manner by radio-frequency (RF) subcarriers, has been suggested as a low-cost, high quality, secure, and reliable technology for aggregating Worldwide Interoperability for Microwave Access (WiMAX) traffic. As an alternative to millimeter-wave links, free-space optical (FSO) backhaul links offer high capacity and use seamless connections to optical fibres when connecting the core network [1]–[6].

Optical wireless technology was considered as a potential distributer of WiMAX traffic in metro or access networks [1], [3]–[6]. Cvijetic *et al.* studied transmission of orthogonal frequency-division

multiplexing (OFDM) WiMAX traffic over FSO link via subcarrier modulation with direct/heterodyne detection in [3] and [4], respectively, where outage and symbol error performance was determined for both detection techniques. In [5], a multiple-input multiple-output architecture for distributing WiMAX traffic using optical wireless technology is presented, where different protocols are considered. A network consisting of a satellite, high altitude platforms and subscribers for WiMAX traffic was proposed in [6], and results indicated that laser links could be a viable technology for providing mobile communication services. Outage probability of WiMAX on FSO was examined by Vaiopolos *et al.* in [1], where the combined effects of link distance, path loss, log-normal shadowing and atmospheric turbulence were analyzed.

In contrast to [1], we extend the analysis to a more general case. Atmospheric turbulence is modeled by the Gamma-Gamma distribution, proven to be an excellent model for weak, moderate and strong atmospheric turbulence conditions [7]–[12], as opposed to a log-normal model [1], which accounts only for weak turbulence. This Gamma-Gamma model has been proved that has experimental support [7]–[12]. Furthermore, multipath fading is modeled by the Nakagami-*m* distribution, allowing the analysis of fading conditions that can have a direct component, as well as severe fading, even more severe than Rayleigh, considered in [1]. Besides multipath fading, the shadowing effect over RF part is also taken into account [13]–[16], and it is modeled by the Gamma distribution whose parameters are linked with shadowing spread. The shadowing effect depends on receiver surroundings and characteristically appears in industrial wireless network environment [13]. This Gamma-shadowed Nakagami-*m* composite fading model was experimentally verified in [17] and [18]. The analysis in this paper is suited for both *M*-ary phase-shift keying (M-PSK) and *M*-ary quadrature amplitude modulation (M-QAM).

In this paper, we investigate the overall outage probability dependence on different simultaneous effects, like optical link length, distance between RF user and base station (BS), modulation scheme and constellation size used, fading and shadowing severity, turbulence conditions, and pointing errors. The FSO apertures are usually deployed on high buildings, and therefore vibrations of the transmitted optical signal caused by building sway, strong wind, or weak earthquakes causes misalignment between the transmitter and the receiver. The pointing error phenomena is therefore also known as misalignment fading [18]–[20]. The goal of this paper is to optimize the laser beam radius at the waist in the presence of Nakagami-*m* multipath fading and Gamma shadowing over the RF part, in order to minimize the outage probability. In addition, using the probability density function (PDF) of received signal-to-noise ratio (SNR), we spread the analysis to determining the overall amount of fading (AF), which is a significant measure of fading severity [5], [21].

The rest of the paper is organized as follows. Section 2 introduces the system model. The outage probability analysis is given in Section 3, for both M-PSK and M-QAM modulation schemes. Section 4 contains the derivation of moments and AF. The simulation model is described in Section 5. Section 6 presents numerical results with appropriate discussions, and concluding remarks are given in Section 7.

2. System Model

We investigate a FSO link used as a WiMAX backhaul, aggregating and delivering traffic from a core network/Internet to the end users. The complex system consists of FSO and RF subsystems. The system model is shown in Fig. 1.

The FSO subsystem uses subcarrier intensity modulation (SIM) [7], [22]–[25]. The laser transmitter aperture which is connected to a core network is mounted on a high building or pole, allowing line-of-sight (LoS) to the WiMAX BS. The aperture is directed at the optical receiver. The received optical signal is fed to the detector, which further converts it to an electrical signal using a PIN photodetector.

The electrical signal is then transmitted to the end users. WiMAX employs OFDM with a large number of orthogonal subcarriers, denoted by *N*. Each subcarrier is modulated either by M-PSK

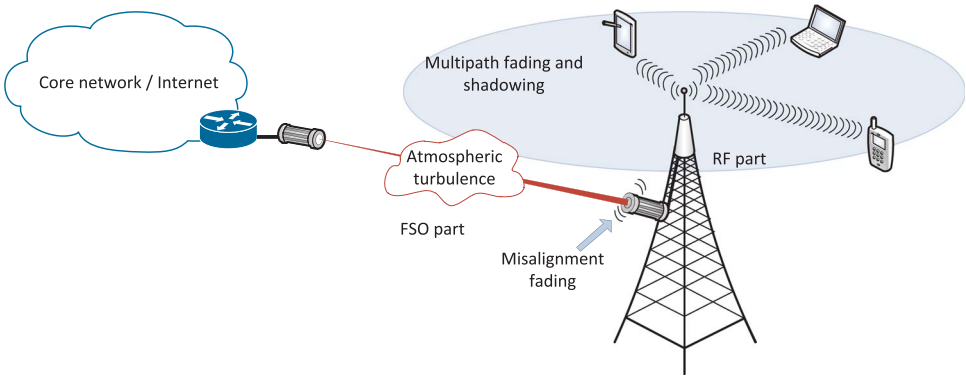

Fig. 1. System model consisting of an FSO backhaul link, connecting a WiMAX base station with the core network/Internet.

or M-QAM scheme. The total received electrical power per end user is obtained by dividing the total electrical power by N.

In the FSO part of the system, the optical signal is damaged by path loss, atmospheric turbulence and pointing errors. The combined channel state h, which incorporates these three terms, is given as

$$h = h_l h_a h_p \tag{1}$$

where h_l denotes atmospheric path loss, h_a is the atmospheric turbulence, and h_p denotes pointing errors. It is assumed that all three terms are independent [18].

Atmospheric path loss is constant during a long time period. Its value is determined by Beers-Lambert Law as [18]

$$h_l = \exp(-\sigma d_O) \tag{2}$$

where d_O is the optical propagation path length, and $\sigma = 0.1$ dB/km is the attenuation coefficient, which is a result of the superposition of multiple scattering and absorption processes [26].

Random changes in atmospheric temperature, pressure, altitude and wind speed can cause variations in the refractive index, leading to the presence of atmospheric turbulence. The received signal is consequently degraded by these intensity fluctuations. The statistical model that has shown to have excellent alignment in both theoretical calculations and empirical measurements for a wide range of turbulence conditions is the Gamma-Gamma distribution. The PDF of the irradiance h_a is given by [7]–[9]

$$f_{h_a}(h_a) = \frac{2(\alpha\beta)^{\frac{\alpha+\beta}{2}}}{\Gamma(\alpha)\Gamma(\beta)} h_a^{\frac{\alpha+\beta}{2}-1} K_{\alpha-\beta}\left(2\sqrt{\alpha\beta h_a}\right) \tag{3}$$

where $\Gamma(\cdot)$ is the Gamma function defined in [27, eq. (8.310.1)], and K_v is the modified Bessel function of the second kind and order v defined in [27, eq. (8.432)]. The parameters α and β represent the effective number of small scale and large scale cells and relate to the atmospheric conditions. Assuming plane-wave propagation and zero inner scale, α and β are given as [7] and [8]

$$\alpha = \left(\exp\left(0.49\sigma_R^2 \Big/ \left(1 + 1.11\sigma_R^{12/5}\right)^{7/6}\right) - 1\right)^{-1} \tag{4}$$

and

$$\beta = \left(\exp\left(0.51\sigma_R^2 \Big/ \left(1 + 0.69\sigma_R^{12/5}\right)^{5/6}\right) - 1\right)^{-1} \tag{5}$$

where $\sigma_R^2 = 1.23 C_n^2 k^{7/6} d_O^{11/6}$ is the Rytov variance, with $k = 2\pi/\lambda_o$, and C_n^2 denotes the weather dependent index of refraction structure.

Due to the LoS requirements, FSO apertures are usually installed on high altitudes. Thermal expansion, weak earthquakes and building sway lead to the vibrations of the transmitted beam. The misalignment between the transmitting and receiving telescope is called misalignment fading or pointing errors. To statistically model pointing errors, we adopt the model which assumes a Gaussian spatial intensity profile of beam radius w_z on the receiver plane, and a circular aperture radius a. Both horizontal and vertical sways are modeled as independent and identically distributed Gaussian random variables with zero mean and standard deviation denoted by σ_S. The radial displacement at the receiver is therefore determined by a Rayleigh distribution. The PDF of the pointing errors can be obtained as [18]

$$f_{h_p}(h_p) = \frac{\gamma^2}{A_0^{\gamma^2}} h_p^{\gamma^2 - 1}, \ 0 \le h_p \le A_0 \tag{6}$$

where $\gamma = w_{zeq}/(2\sigma_S)$ is the ratio between the equivalent laser beam waist and the pointing error standard deviation, with $w_{zeq}^2 = w_z^2 \sqrt{\pi} \times \text{erf}(v)/2v\exp(-v^2)$; $v = \sqrt{\pi} a/\sqrt{2} w_z$, w_z is the beam waist on the receiver plane; $A_0 = [\text{erf}(v)]^2$ is the fraction of the collected received optical power at $d_O = 0$; and erf$(\cdot)$ is the error function defined in [27, eq. (8.250.1)]. Furthermore, the beam radius at the distance d_O, w_z is related to beam radius at the waist denoted as w_0 and to the radius of curvature denoted as F_0, as [28] $w_z = w_0 \sqrt{((\Theta_o + \Lambda_o)(1 + 1.63\sigma_R^{12/5}\Lambda_1))}$, where $\Theta_o = 1 - (d_O/F_0)$, $\Lambda_o = 2d_O/kw_z^2$, and $\Lambda_1 = \Lambda_o/(\Theta_o^2 + \Lambda_o^2)$.

The resulting PDF of

$$H = h_a h_p \tag{7}$$

is obtained as [18]

$$f_H(H) = \frac{\gamma^2 \alpha\beta}{A_0 \Gamma(\alpha)\Gamma(\beta)} \times G_{1,3}^{3,0}\left(\frac{\alpha\beta}{A_0} H \Big| \begin{matrix} \gamma^2 \\ \gamma^2 - 1, \quad \alpha - 1, \quad \beta - 1 \end{matrix}\right) \tag{8}$$

where $G_{p,q}^{m,n}(\cdot)$ is the Meijer's G-function defined in [27, eq. (9.301)].

The received optical power at the BS can be determined by the Friis transmission equation as [29]

$$P_{R-O} = P_{T-O} n_T n_R G_{T-O} G_{R-O} \left(\frac{\lambda_o}{4\pi d_O}\right)^2 h \tag{9}$$

where P_{R-O}, n_R and G_{R-O} are the optical power, efficiency and telescope gain at the receiver, while P_{T-O}, n_T and G_{T-O} are the optical power, efficiency and telescope gain at the transmitter.

The optical power is multiplied by a constant K_{O-RF} and then converted to RF using a square-law device [6]

$$P_{T-RF} = K_{O-RF} (P_{R-O})^2. \tag{10}$$

The path loss between the BS and a wireless user is determined by a simple model, which is a function of distance [14]. The received RF signal power is given by

$$P_{R-RF} = P_{T-RF} \left(\frac{\lambda_{RF}\sqrt{G_l}}{4\pi d_{RF0}}\right)^2 \left(\frac{d_{RF0}}{d_{RF}}\right)^{\nu} \tag{11}$$

where P_{R-RF} is the received power by the user, P_{T-RF} is the transmitted power by the BS, λ_{RF} is the RF signal wavelength, $\sqrt{G_l}$ is the product of the RF transmitted and received antenna field patterns in the LoS direction, d_{RF0} is a reference distance for the antenna far field, d_{RF} is the distance between the RF transmitter and the user, and ν is the RF path loss exponent.

The RF transmitted power per WiMAX subcarrier is obtained by dividing (10) by the number of subcarriers N as

$$P_{T-RF,sub} = \frac{P_{T-RF}}{N}. \tag{12}$$

The overall received RF power per a wireless user, including path loss, multipath fading and shadowing is obtained as

$$P_{R-RF,sub} = P_{T-RF,sub}\left(\frac{\lambda_{RF}\sqrt{G_l}}{4\pi d_{RFO}}\right)^2\left(\frac{d_{RFO}}{d_{RF}}\right)^{\nu}\rho \tag{13}$$

where ρ is the random variable associated with the squared envelope of a composite wireless channel subject to multipath fading and shadowing.

In wireless communications, both short-term (multipath) and long-term fading (shadowing) occur simultaneously. Multipath fading models the superposition of delayed, reflected, scattered and diffracted signal components, while shadowing models the local topography in the receiver surroundings [14]–[17]. The multipath part of the composite fading channel can be described by the Nakagami-m distribution, and the shadowing part can be described by the log-normal distribution. This composite model is not suitable for mathematical manipulation, and log-normal shadowing is replaced by a Gamma distribution with corresponding parameters [15], [16]. This model is known in literature as the Generalized-$\mathcal{K}$ (GK) fading channel [17].

The PDF of the GK fading envelope is given by [16]

$$f_u(u) = \frac{4(mm_s)^{\frac{m+m_s}{2}}u^{m+m_s-1}}{\Gamma(m)\Gamma(m_s)}K_{m_s-m}(2u\sqrt{mm_s}) \tag{14}$$

where $m \geq 0.5$ and $m_s > 0$ are the severity parameters of multipath fading an shadowing, respectively. Smaller values of m account for deeper fading, and smaller values of m_s account for sharper shadowing conditions. When $0.5 \leq m \leq 1$, the multipath fading is even deeper than Rayleigh, which is obtained by setting $m = 1$. When $m > 1$, the propagation environment corresponds to the case when there exists a direct component. The shadowing severity parameter m_s is related to the shadowing spread σ_{SH} in log-normal shadowing as [15]

$$\sigma_{SH}(\text{dB}) = \frac{10}{\ln 10}\sqrt{\psi'(m_s)} \tag{15}$$

where $\psi'(\cdot)$ is the first derivative of the digamma function, defined in [27, eq. (8.360)]. Some experimental results relating multipath fading severity and shadowing spread are available in [17] and [18].

The PDF of the squared envelope $\rho = u^2$ can be obtained by using a RV transform as [16]

$$f_\rho(\rho) = \frac{2(mm_s)^{\frac{m+m_s}{2}}\rho^{\frac{m+m_s}{2}-1}}{\Gamma(m)\Gamma(m_s)}K_{m_s-m}(2\sqrt{\rho mm_s}). \tag{16}$$

After substituting (9) and (10) in (13) and using (1), the received RF power is given as

$$P_{R-RF,sub} = \mathcal{A}\omega \tag{17}$$

where

$$\mathcal{A} = \frac{K_{O-RF}}{N}\left(P_{T-O}n_T n_R\left(\frac{\lambda_o}{4\pi d_o}\right)^2 G_{T-O}G_{R-O}h_l\right)^2 \times \left(\frac{\lambda_{RF}\sqrt{G_l}}{4\pi d_{RFO}}\right)^2\left(\frac{d_{RFO}}{d_{RF}}\right)^{\nu} \tag{18}$$

and

$$\omega = H^2\rho. \tag{19}$$

The PDF of $\theta = H^2$ is obtained by applying a simple random variable transformation $f_\theta(\theta) = (f_H(H)/|\partial\theta/\partial H|)|_{H=\sqrt{\theta}}$, [30, eq. (5–16)] and further simplified using [31, eq. (07.34.16.0001.01)], resulting in

$$f_\theta(\theta) = \frac{\gamma^2}{2\Gamma(\alpha)\Gamma(\beta)}\theta^{-1}G_{1,3}^{3,0}\left(\frac{\alpha\beta}{A_0}\sqrt{\theta}\,\middle|\, \begin{matrix}\gamma^2+1\\ \gamma^2,\ \alpha,\ \beta\end{matrix}\right). \tag{20}$$

Next, we determine the PDF of $\omega = \theta\rho$ as [30]

$$f_\omega(\omega) = \int f_{\omega|\theta}(\omega|\theta)f_\theta(\theta)d\theta \tag{21}$$

where the conditional PDF is obtained as

$$\begin{aligned} f_{\omega|\theta}(\omega|\theta) &= \frac{1}{\theta}f_\rho\left(\frac{\omega}{\theta}\right) \\ &= \frac{2(mm_s)^{\frac{m+m_s}{2}}}{\theta\Gamma(m)\Gamma(m_s)}\left(\frac{\omega}{\theta}\right)^{\frac{m+m_s}{2}-1}K_{m_s-m}\left(2\sqrt{\frac{\omega mm_s}{\theta}}\right). \end{aligned} \tag{22}$$

Inserting (20) and (22) in (21), we obtain

$$\begin{aligned} f_\omega(\omega) = \frac{\gamma^2(mm_s)^{\frac{m+m_s}{2}}\omega^{\frac{m+m_s}{2}-1}}{\Gamma(\alpha)\Gamma(\beta)\Gamma(m)\Gamma(m_s)} \times \int_0^\infty \theta^{-\frac{m+m_s}{2}-1}K_{m_s-m}\left(2\sqrt{\frac{\omega mm_s}{\theta}}\right) \\ \times G_{1,3}^{3,0}\left(\frac{\alpha\beta}{A_0}\sqrt{\theta}\,\middle|\, \begin{matrix}\gamma^2+1\\ \gamma^2,\ \alpha,\ \beta\end{matrix}\right)d\theta. \end{aligned} \tag{23}$$

Using [31, eq. (03.04.26.0009.01)], we can express the modified Bessel function in terms of the Meijer's G-function and, afterwards, transform it into a more desirable form using [31, eq. (07.34.16.0002.01)] as

$$K_{m_s-m}\left(2\sqrt{\frac{\omega mm_s}{\theta}}\right) = \frac{1}{2}G_{2,0}^{0,2}\left(\frac{\theta}{\omega mm_s}\,\middle|\, \begin{matrix}\chi_1\\ -\end{matrix}\right). \tag{24}$$

For better visibility, the parameters in the G-function in (24) are grouped as

$$\chi_1 = 1 - \frac{m_s - m}{2},\quad 1 - \frac{m - m_s}{2}. \tag{25}$$

Replacing (24) in (23), $f_\omega(\omega)$ is expressed as

$$\begin{aligned} f_\omega(\omega) = \frac{\gamma^2(mm_s)^{\frac{m+m_s}{2}}\omega^{\frac{m+m_s}{2}-1}}{2\Gamma(\alpha)\Gamma(\beta)\Gamma(m)\Gamma(k)} \times \int_0^\infty \theta^{-\frac{m+m_s}{2}-1}G_{2,0}^{0,2}\left(\frac{\theta}{\omega mm_s}\,\middle|\, \begin{matrix}\chi_1\\ -\end{matrix}\right) \\ \times G_{1,3}^{3,0}\left(\frac{\alpha\beta}{A_0}\sqrt{\theta}\,\middle|\, \begin{matrix}\gamma^2+1\\ \gamma^2,\ \alpha,\ \beta\end{matrix}\right)d\theta. \end{aligned} \tag{26}$$

The integral in (26) can be solved using [31, eq. (07.34.21.0013.01)] as

$$f_{\omega}(\omega) = \frac{\gamma^2 2^{\alpha+\beta-3}}{\pi\Gamma(\alpha)\Gamma(\beta)\Gamma(m)\Gamma(m_s)\omega} \times G_{2,8}^{8,0}\left(\frac{\alpha^2\beta^2 m m_s \omega}{16{A_0}^2}\middle| \begin{matrix}\chi_2\\ \chi_3\end{matrix}\right) \tag{27}$$

with

$$\chi_2 = \frac{\gamma^2+1}{2}, \quad \frac{\gamma^2+2}{2} \tag{28}$$

and

$$\chi_3 = \frac{\gamma^2}{2}, \quad \frac{\gamma^2+1}{2}, \quad \frac{\alpha}{2}, \quad \frac{\alpha+1}{2}, \quad \frac{\beta}{2}, \quad \frac{\beta+1}{2}, \quad m_s, \quad m. \tag{29}$$

Finally, the order of the Meijer's *G*-function can be reduced with the help of [31, eq. (07.34.03. 0002.01)], resulting in

$$f_{\omega}(\omega) = \frac{\gamma^2 2^{\alpha+\beta-3}}{\pi\Gamma(\alpha)\Gamma(\beta)\Gamma(m)\Gamma(m_s)\omega} \times G_{1,7}^{7,0}\left(\frac{(\alpha\beta)^2 m m_s \omega}{16{A_0}^2}\middle| \begin{matrix}\xi_1\\ \kappa_1\end{matrix}\right) \tag{30}$$

where

$$\xi_1 = 1 + \frac{\gamma^2}{2} \tag{31}$$

and

$$\kappa_1 = \frac{\gamma^2}{2}, \quad \frac{\alpha}{2}, \quad \frac{\alpha+1}{2}, \quad \frac{\beta}{2}, \quad \frac{\beta+1}{2}, \quad m_s, \quad m. \tag{32}$$

The CDF of ω is obtained by taking the integral $F_{\omega}(W) = \int_0^W f_{\omega}(\omega)d\omega$ and can be solved using [31, eq. (07.34.21.0084.01)] as

$$F_{\omega}(W) = \frac{\gamma^2 2^{\alpha+\beta-3}}{\pi\Gamma(\alpha)\Gamma(\beta)\Gamma(m)\Gamma(m_s)} \times G_{2,8}^{7,1}\left(\frac{m m_s (\alpha\beta)^2 W}{16A_0^2}\middle| \begin{matrix}\xi_2\\ \kappa_2\end{matrix}\right) \tag{33}$$

with

$$\xi_2 = 1, \quad 1 + \frac{\gamma^2}{2} \tag{34}$$

and

$$\kappa_2 = \frac{\gamma^2}{2}, \quad \frac{\alpha}{2}, \quad \frac{\alpha+1}{2}, \quad \frac{\beta}{2}, \quad \frac{\beta+1}{2}, \quad m_s, \quad m, \quad 0. \tag{35}$$

To the best of the authors' knowledge, the derived closed-form expressions for PDF and CDF in (30) and (33) are novel and can be utilized in determining different performance metrics. It should be noted that both PDF and CDF are expressed in terms of Meijer's *G*-functions that are the standard built-in functions in Mathematica software package. In addition, Meijer's *G*-functions can be transformed in more familiar hypergeometric functions [27, eq. (9.41.1)] by applying the relation [31, eq. (07.34.26.0004.01)]. Through the use of (33), we obtain the outage probability for our analysis.

3. Outage Probability Analysis

An outage event occurs when the received power for a WiMAX user falls below a predetermined minimum power level. Hence, the outage probability is

$$\mathcal{P}_{O,sub} = \Pr(P_{R-RF,sub} < P_{\min,sub}) \tag{36}$$

where $\Pr(\cdot)$ denotes probability, and $P_{\min,sub}$ is the minimum power level. Combining (17) and (36), we can express the outage probability as

$$\mathcal{P}_{O,sub} = \Pr\left(\omega < \frac{P_{\min,sub}}{\mathcal{A}}\right). \tag{37}$$

As stated in the previous section, we use the CDF of ω given by (33) to obtain the outage probability $\mathcal{P}_{O,sub}$ as

$$\mathcal{P}_{O,sub} = F_{\omega}\left(\frac{P_{\min,sub}}{\mathcal{A}}\right). \tag{38}$$

To estimate the minimum power level $P_{\min,sub}$, we assume that each subcarrier is modulated by BPSK, M-PSK or M-QAM scheme.

If each subcarrier is BPSK modulated, the bit error rate can be estimated by the well-known equation [32]

$$\mathcal{P}^{BPSK}_{BER,sub} = 0.5\text{erfc}(\sqrt{SNR}) \tag{39}$$

where $SNR = P_s T_s/(N_{RF} + N_O)$ is the average symbol SNR [6]; P_s is the average symbol power; T_s is the symbol duration; N_{RF} and N_O are the noise power densities of the RF and optical receivers, respectively; while $\text{erfc}(x)$ denotes the complementary error function defined in [27, eq. (8.250.4)]. From (39), by setting $P^{BPSK}_{\min,sub} = P_s$, the minimum required power for BPSK signals is obtained as

$$P^{BPSK}_{\min,sub} = \frac{(N_{RF} + N_O)\left[\text{erfc}^{-1}\left(2\mathcal{P}^{BPSK}_{BER,sub}\right)\right]^2}{T_s}. \tag{40}$$

Moreover, if each subcarrier is M-PSK modulated, an approximation for the symbol error rate for large M is given as [32]

$$\mathcal{P}^{MPSK}_{SER,sub} \approx 2Q\left(\sqrt{2SNR}\sin\left(\frac{\pi}{M}\right)\right) \tag{41}$$

where $Q(\cdot)$ denotes the well-known Gaussian Q function. Using the relation $\text{erfc}(x) = 2Q(\sqrt{2}x)$, $P^{MPSK}_{\min,sub}$ for a target $\mathcal{P}^{MPSK}_{SER,sub}$ is obtained as

$$P^{MPSK}_{\min,sub} \approx \frac{(N_{RF} + N_O)\left[\text{erfc}^{-1}\left(\frac{\mathcal{P}^{MPSK}_{SER,sub}}{2}\right)\right]^2}{T_s \sin^2\left(\frac{\pi}{M}\right)}. \tag{42}$$

The upper bound for M-QAM symbol error rate can be found as [1], [32]

$$\mathcal{P}^{MQAM}_{SER,sub} \leq 4Q\left(\sqrt{3SNR/(M-1)}\right) \tag{43}$$

Following the same steps as in the BPSK and M-PSK schemes, the minimum required power for M-QAM can be obtained as [1]

$$P_{\min,sub}^{MQAM} \leq \frac{2(N_{RF}+N_O)(M-1)\left[\text{erfc}^{-1}\left(\frac{\mathcal{P}_{SER,sub}^{MQAM}}{2}\right)\right]^2}{3T_s}. \tag{44}$$

4. Moments and AF

The amount of fading is a measure of fading severity and can be computed on the basis of the first two moments of the received SNR. This measure was originally introduced by Charash in [21] and frequently used in performance analysis of wireless channels, e.g., [5].

The n-th moment of the received power defined as $\mathrm{E}[(\mathcal{A}\omega)^n] = \mathcal{A}^n \int_0^\infty \omega^n f_\omega(\omega) d\omega$ can be expressed as

$$\mathrm{E}\left[(\mathcal{A}\omega)^n\right] = \frac{\gamma^2 2^{\alpha+\beta-3}}{\pi\Gamma(\alpha)\Gamma(\beta)\Gamma(m)\Gamma(m_s)\Gamma(n+1+\gamma^2/2)} \times \left(\frac{16A_0^2\mathcal{A}}{(\alpha\beta)^2 m m_s}\right)^n \prod_{k=1}^{7}\Gamma(n+b_k) \tag{45}$$

where b_k are the individual values of κ_1.

The amount of fading is expressed in terms of moments as $AF_\omega = \mathrm{E}[(\mathcal{A}\omega)^2]/\mathrm{E}[\mathcal{A}\omega]^2 - 1$. Directly from (45), the expression for AF is obtained as

$$AF_\omega = \frac{\pi\Gamma(\alpha)\Gamma(\beta)\Gamma(m)\Gamma(m_s)\Gamma(2+\gamma^2/2)^2}{\gamma^2 2^{\alpha+\beta-3}\Gamma(3+\gamma^2/2)} \times \prod_{k=1}^{7}\frac{\Gamma(n+b_k)}{\Gamma(1+b_k)^2} - 1. \tag{46}$$

The AF is the measure of random process fluctuations with respect to its mean value.

5. Simulation Model

Monte-Carlo simulations were performed using MATLAB software package by generating 10^7 random variables (RVs) which are associated with the mixed FSO/WiMAX model. All commands for generating RVs are built-in into MATLAB. The RV which follows the Gamma-Gamma distribution is generated as a product of two independent Gamma-distributed RVs with shaping parameters α and β, respectively. In a similar fashion, the GK RV is generated as a product of the square root of two independent Gamma-distributed RVs with shaping parameters m and m_s, respectively, where m_s is related to the shadowing spread as given in (15). Finally, the RV associated with the mixed FSO/WiMAX model is obtained based on (7) and (9). The generated RV ω is then compared to the predetermined threshold. Outage probability is finally obtained by counting how many times the generated mixed FSO/WiMAX RV is less than the threshold.

6. Numerical Results

Using the expression for the outage probability, we present numerical results to investigate the different effects of the parameters of RF and FSO subsystems on outage probability. Furthermore, we determine the optimum beam radius at the waist, which minimizes outage probability. All analytical results are confirmed by Monte-Carlo simulations.

In all figures, plotted curves are based on the equations derived in Section 3, while red dots correspond to the Monte-Carlo simulations with appropriate parameters. The values of WiMAX and FSO parameters, unless otherwise stated in the figures, are taken from [1] and are given in Table 1. Both analytical and simulation results are obtained on the same computer, equipped with third generation Intel i7 processor with eight threads and 32 gigabytes of RAM. A single point obtained analytically is calculated at an average of 0.038 seconds using Mathematica software package. A single point obtained by means of Monte-Carlo simulation for 10^7 generated RVs using MATLAB is calculated at an average of 1506.39 seconds. Performance evaluation

TABLE 1

Numerical parameters for the mixed FSO/WiMAX link, similar to [1]

Parameter	Symbol	Value
Optical power at the transmitter	P_{T-O}	40 mW
Optical transmitter telescope gain	G_{T-O}	72 dB
Optical receiver telescope gain	G_{R-O}	112 dB
Optical transmitter efficiency	n_T	0.9
Optical receiver efficiency	n_R	0.9
Optical signal wavelength	λ_O	1550 nm
Ratio between the RF power and the square of the optical power	K_{O-RF}	110 dB
Product of the transmit and receive antenna field	$\sqrt{G_l}$	44.7 dB
RF signal reference distance	d_{RFO}	100 m
RF path loss	ν	3.5
RF signal wavelength	λ_{RF}	8.57×10^{-2} m
Noise power density of the optical receiver	N_O	10^{-22} W/Hz
Noise power density of the RF receiver	N_{RF}	5×10^{-19} W/Hz
Number of sub-carriers in a channel	N	1024
Symbol duration	T_s	0.1024 μs
Target symbol error rate	$\mathcal{P}_{SER,sub}$	10^{-6}

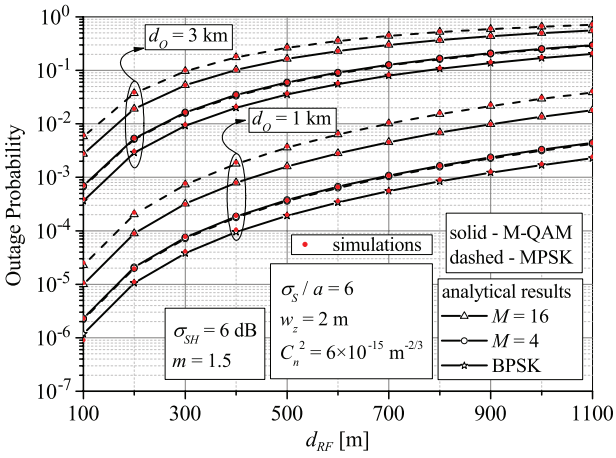

Fig. 2. Outage probability dependence on RF-link distance for different modulation schemes. Multi-path fading and shadowing are moderate, and atmospheric turbulence is weak.

based on analytical expressions is about 4×10^4 times faster than that based on Monte-Carlo simulations.

Outage probability dependence on RF link distance, d_{RF}, (WiMAX BS—end user) for different modulation schemes is presented in Fig. 2. On the basis of the expressions derived here, it is possible to calculate outage probability when different modulations are used over different FSO and WiMAX link lengths. As expected, outage probability increases as the optical and RF link distances increase. In addition to constellation sizes of $M = 4$ and $M = 16$, BPSK curves are plotted as well, which, as expected, give the best performance. For a constellation size of $M = 4$, QAM and PSK schemes give the same results. As for higher modulation schemes, e.g., $M = 16$, switching from PSK to QAM will result in better performance. Increasing the optical link

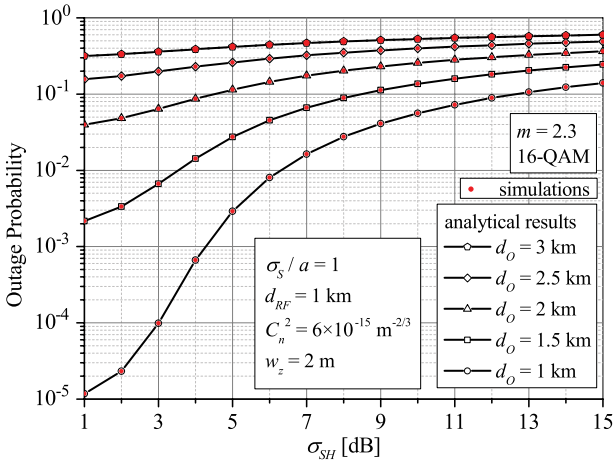

Fig. 3. Outage probability dependence on shadowing spread for different values of optical link length and weak turbulence.

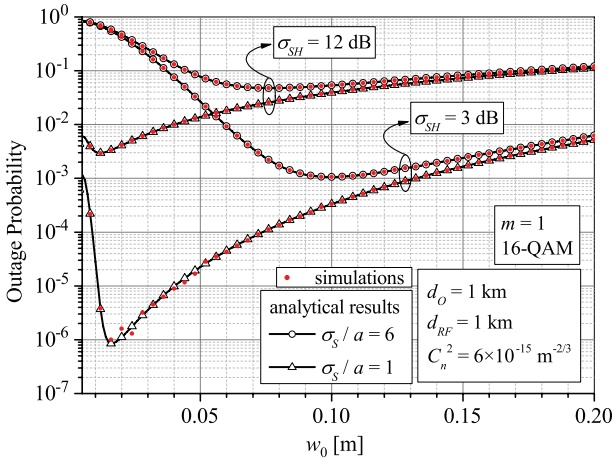

Fig. 4. Outage probability dependence on beam radius at the waist in Rayleigh fading and weak turbulence for different values of shadowing severity and jitter variance.

distance from 1 km to 3 km will not only deteriorate the outage probability in the whole range of d_{RF} but will also decrease the performance gap when switching from QAM to PSK at greater RF distance.

The effect of shadowing is shown in Fig. 3. For shorter optical links, shadowing will have a greater impact on outage probability. For instance, as σ_{SH} increases from 2 dB to 12 dB, outage probability increases from 2.3×10^{-5} to 0.09 for $d_O = 1$ km but only from 0.33 to 0.571 for $d_O = 3$ km.

The optimization of the transmitter laser beam radius at the waist is presented in Figs. 4–6. Outage probability dependence on beam waist at the transmitter in different fading and shadowing conditions is presented in Figs. 4 and 5, while the impact of different turbulence conditions on optimal beam radius at the waist is shown in Fig. 6. We examine the results and present which values of w_0, denoted as w_{opt} minimizes the outage probability.

Fig. 4 shows outage probability dependence on w_0 in different shadowing conditions and for different values of normalized jitter standard deviation. When the normalized jitter standard deviation σ_S/a is equal to one, the optimum w_0, which minimizes the outage, remains around $w_{opt} =$ 1.2 cm for both light and heavy shadowing. However, when $\sigma_S/a = 6$, this optimum value shifts from 7.7 cm at $\sigma_{SH} = 3$ dB to 9.4 cm at $\sigma_{SH} = 12$ dB. The greater the value of normalized jitter

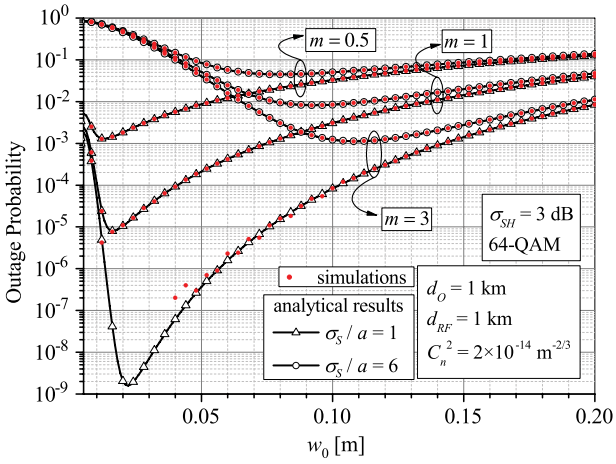

Fig. 5. Outage probability dependence on beam radius at the waist in light shadowing and moderate turbulence for different values of fading severity and jitter variance.

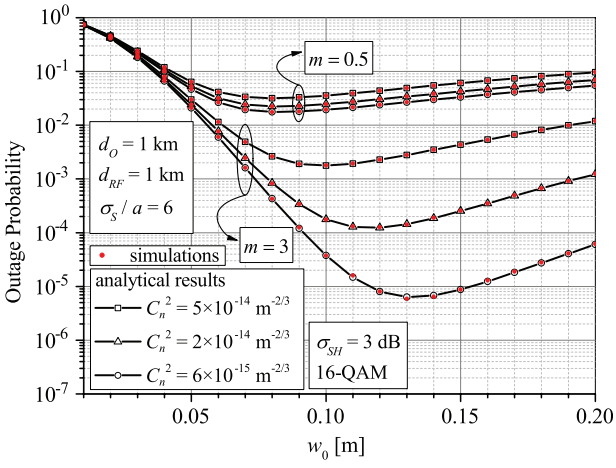

Fig. 6. Outage probability dependence on beam radius at the waist in light shadowing for different values of fading severity and turbulence conditions.

standard deviation, the stronger is the effect of σ_{SH} on w_{opt}. When shadowing spread is lower, the minimum value of outage probability varies for three orders of magnitude, while when σ_{SH} is 12 dB, it varies only for an order of magnitude.

Multipath fading severity has a similar effect as shadowing when choosing the optimal w_0, as it is shown in Fig. 5. The optimum beam radius at the waist has almost remains the same in deep and shallow fading conditions when $\sigma_S/a = 1$. As this ratio is increased, i.e., misalignment is greater, w_{opt} increases as fading conditions improve from $m = 0.5$ to $m = 3$. The optimal value of laser beam radius at the waist decreases as multipath fading severity increases. The multipath fading severity parameter has greater effect on w_{opt} when normalized jitter standard deviation is greater.

Finally, the influence of atmospheric turbulence on optimal value of beam radius at the waist is shown in Fig. 6. In contrast to [1], where the log-normal distribution is used to model only weak atmospheric turbulence, we observe the additional effects of both moderate and heavy turbulence conditions on the optimal value of beam radius at the waist. The change in turbulence conditions have weak influence on outage probability in very deep multipath fading, where weak turbulence only slightly improves outage compared to strong turbulence. Since multipath

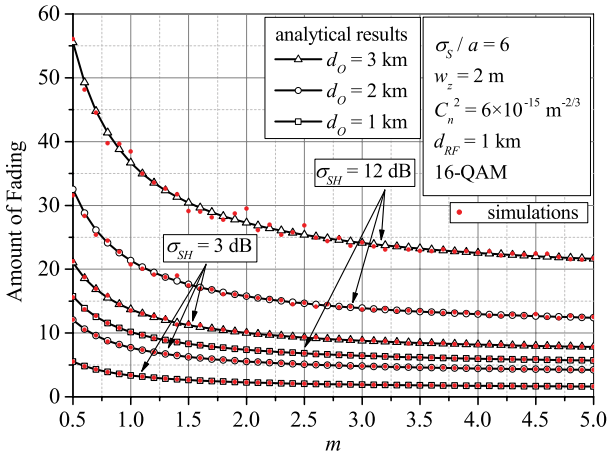

Fig. 7. Amount of fading dependence on fading severity for different values of shadowing spread and optical link length.

fading is modeled by the Nakagami-m distribution, we observe this outage minimum not only for the case when there is no direct component (as in Rayleigh fading) but for scenarios where there exists a direct component as well, which accounts for real-world scenarios. As multipath fading conditions improve, for optimal value of beam radius at the waist, outage is decreased by several orders of magnitude when compared to strong conditions. For $m = 0.5$, fading is more severe than the Rayleigh case, and outage probability has a minimum at around $w_0 = 0.8$ cm for all turbulence conditions. On the other hand, for $m = 3$, this minimum varies and is obtained at 13 cm, 12 cm and 10 cm for weak, moderate and strong turbulence conditions, respectively.

The AF dependence on fading severity m for different values of shadowing spread and optical link length is shown in Fig. 7. As expected, the AF decreases as fading severity parameter m increases, for all shadowing sharpness and link distance. Sharper shadowing conditions increases the AF, and for instance, at $m = 1$ and $d_O = 1$ km, AF is only 3.47 for $\sigma_{SH} = 3$ dB, and 10.11 for $\sigma_{SH} = 12$ dB. This effect is more apparent at larger optical link length, and for the same multipath fading severity and $d_O = 3$ km, the AF increases from 13.62 to 36.61 as shadowing spread increases from 3 to 12 dB.

7. Conclusion

In this paper, we have derived novel analytical expressions for overall outage probability of a hybrid FSO/WiMAX system and confirmed numerical results with Monte-Carlo simulations. We have analyzed the outage performance dependence on RF and FSO link distance, turbulence, shadowing and fading. After that, the optimization of laser beam radius at the waist has been performed under the condition of minimal value of the outage probability. The results have illustrated that by changing shadowing spread over RF link from 2 dB to 15 dB, the overall outage probability could be increased significantly, even for four orders of magnitude. In addition, the outage probability can be improved by several orders of magnitude by proper selection of laser beam radius at the waist. On the basis of the results, the conclusion is that the effect of optimal selection of laser beam radius at the waist on outage probability becomes stronger with decreasing of misalignment and turbulence strength over FSO link, as well as with decreasing of shadowing spread and multipath fading severity over RF link.

Acknowledgment

The authors would like to thank the reviewers and the associate editor for the valuable comments that improved the quality of this paper.

References

[1] N. Vaiopoulos, H. Sandalidis, and D. Varoutas, "WiMAX on FSO: Outage probability analysis," *IEEE Trans. Commun.*, vol. 60, no. 10, pp. 2789–2795, Oct. 2012.

[2] P. T. Dat *et al.*, "Investigation of suitability of RF signal transmission over FSO links," in *Proc. HONET*, Nov. 2007, pp. 1–6.

[3] N. Cvijetic, S. Wilson, and C. Brown, "WiMAX access using optical wireless technology with heterodyne detection in turbulent atmospheric channels," in *Proc. IEEE GLOBECOM*, Nov. 2006, pp. 1–5.

[4] N. Cvijetic and T. Wang, "WiMAX over free-space optics-evaluating OFDM multi-subcarrier modulation in optical wireless channels," in *Proc. IEEE Sarnoff Symp.*, Mar. 2006, pp. 1–4.

[5] N. Cvijetic and T. Wang, "A MIMO architecture for IEEE 802.16d (WiMAX) heterogeneous wireless access using optical wireless technology," in *Next Generation Teletraffic and Wired/Wireless Advanced Networking*, vol. 4003, Lecture Notes in Computer Science, Y. Koucheryavy, J. Harju, and V. Iversen, Eds. Berlin, Germany: Springer-Verlag, 2006, pp. 441–451.

[6] S. Arnon, "Minimization of outage probability of WiMAX link supported by laser link between a high-altitude platform and a satellite," *J. Opt. Soc. Amer. A, Opt. Image Sci.*, vol. 26, no. 7, pp. 1545–1552, Jul. 2009.

[7] Z. Ghassemlooy, W. Popoola, and S. Rajbhandari, *Optical Wireless Communications: System and Channel Modelling With MATLAB*. Boca Raton, FL, USA: CRC, 2012.

[8] L. C. Andrews and R. L. Phillips, *Laser Beam Propagation Through Random Media*. Bellingham, WA, USA: SPIE, 2005.

[9] E. Zedini, I. Ansari, and M.-S. Alouini, "Performance analysis of mixed Nakagami-*m* and Gamma–Gamma dual-hop FSO transmission systems," *IEEE Photon. J.*, vol. 7, no. 1, Feb. 2015, Art. ID 7900120.

[10] J. Perez, S. Zvanovec, Z. Ghassemlooy, and W. O. Popoola, "Experimental characterization and mitigation of turbulence induced signal fades within an ad hoc FSO network," *Opt. Exp.*, vol. 22, no. 3, pp. 3208–3218, Feb. 2014.

[11] J. Libich and S. Zvanovec, "Influences of turbulences in near vicinity of buildings on free-space optical links," *IET Microw. Antennas Propag.*, vol. 5, no. 9, pp. 1039–1044, Jun. 2011.

[12] D. T. Wayne *et al.*, "Comparing the log-normal and gamma–gamma model to experimental probability density functions of aperture averaging data," in *Proc. SPIE Free-Space Laser Commun. X*, Aug. 2010, p. 78140K1.

[13] E. Tanghe *et al.*, "The industrial indoor channel: Large-scale and temporal fading at 900, 2400, and 5200 MHz," *IEEE Trans. Wireless Commun.*, vol. 7, no. 7, pp. 2740–2751, Jul. 2008.

[14] A. Goldsmith, *Wireless Communications*. Cambridge, U.K.: Cambridge Univ. Press, 2005.

[15] P. Shankar, "Error rates in generalized shadowed fading channels," *Wireless Pers. Commun.*, vol. 28, no. 3, pp. 233–238, Feb. 2004.

[16] I. Kostic, "Analytical approach to performance analysis for channel subject to shadowing and fading," *Proc. Inst. Elect. Eng.—Commun*, vol. 152, no. 6, pp. 821–827, Dec. 2005.

[17] K. Peppas, G. Alexandropoulos, C. Datsikas, and F. Lazarakis, "Multivariate gamma–gamma distribution with exponential correlation and its applications in radio frequency and optical wireless communications," *IET Microw. Antennas Propag.*, vol. 5, no. 3, pp. 364–371, Feb. 2011.

[18] T. Chrysikos, G. Georgopoulos, and S. Kotsopoulos, "Empirical calculation of shadowing deviation for complex indoor propagation topologies at 2.4 GHz," in *Proc. ICUMT*, Oct. 2009, pp. 1–6.

[19] S. Arnon, "Effects of atmospheric turbulence and building sway on optical wireless-communication systems," *Opt. Lett.*, vol. 28, no. 2, pp. 129–131, Jan. 2003.

[20] H. Sandalidis, T. Tsiftsis, and G. Karagiannidis, "Optical wireless communications with heterodyne detection over turbulence channels with pointing errors," *J. Lightw. Technol.*, vol. 27, no. 20, pp. 4440–4445, Oct. 2009.

[21] U. Charash, "Reception through Nakagami fading multipath channels with random delays," *IEEE Trans. Commun.*, vol. COMM-27, no. 4, pp. 657–670, Apr. 1979.

[22] P. Wang *et al.*, "Average BER of subcarrier intensity modulated free space optical systems over the exponentiated Weibull fading channels," *Opt. Exp.*, vol. 22, no. 17, pp. 20828–20841, Aug. 2014.

[23] N. Chatzidiamantis, A. Lioumpas, G. Karagiannidis, and S. Arnon, "Adaptive subcarrier PSK intensity modulation in free space optical systems," *IEEE Trans. Commun.*, vol. 59, no. 5, pp. 1368–1377, May 2011.

[24] W. O. Popoola, Z. Ghassemlooy, J. Allen, E. Leitgeb, and S. Gao, "Free-space optical communication employing subcarrier modulation and spatial diversity in atmospheric turbulence channel," *IET Optoelectron.*, vol. 2, no. 1, pp. 16–23, Feb. 2008.

[25] M. Niu, X. Song, J. Cheng, and J. F. Holzman, "Performance analysis of coherent wireless optical communications with atmospheric turbulence," *Opt. Exp.*, vol. 20, no. 6, pp. 6515–6520, Mar. 2012.

[26] B. T. Vu, N. T. Dang, T. C. Thang, and A. T. Pham, "Bit error rate analysis of rectangular QAM/FSO systems using an APD receiver over atmospheric turbulence channels," *J. Opt. Commun. Netw.*, vol. 5, no. 5, pp. 437–446, May 2013.

[27] I. Gradshteyn and I. Ryzhik, *Table of Integrals, Series, and Products*, 5th ed. San Diego, CA, USA: Academic, 1994.

[28] A. A. Farid and S. Hranilovic, "Outage capacity for MISO intensity-modulated free-space optical links with misalignment," *J. Opt. Commun. Netw.*, vol. 3, no. 10, pp. 780–789, Oct. 2011.

[29] S. Arnon, "Optimization of urban optical wireless communication systems," *IEEE Trans. Wireless Commun.*, vol. 2, no. 4, pp. 626–629, Jul. 2003.

[30] A. Papoulis and S. U. Pillai, *Probability, Random Variables, and Stochastic Processes*. New York, NY, USA: McGraw-Hill, 2002.

[31] *The Wolfarm Functions Site*. [Online]. Available: http://functions.wolfram.com/

[32] J. G. Proakis and M. Salehi, *Digital Communications*. New York, NY, USA: McGraw-Hill, 2008.